Electronic Supplementary Information

Real time optical monitoring of cascade mechanochemical reaction and capture of ultra-unstable intermediate under hydrostatic pressure

Xing Su,[a,b,d] Li Nan,[c] Kai Wang,[c,e] Qian Li,[e] Weiguang Shao,[d] Lulu Liu,[a] Binhong Yu,[a] Yu-Mo Zhang,[a] Tingting Lin,*[b] Bo Zou,*[c] Yifei Liu*[a] and Sean Xiao-An Zhang[a]

[a] College of Chemistry, Jilin University, Changchun 130012, P. R. China

[b] College of Instrumentation and Electrical Engineering, Jilin University, Changchun 130061, P. R. China

[c] State Key Laboratory of Superhard Materials, Jilin University, Changchun 130012, P. R. China

[d] Institute of Systems Engineering, Academy of Military Science, Beijing 102399, P. R. China

[e] Shandong Key Laboratory of Optical Communication Science and Technology, School of Physics Science and Information Technology, Liaocheng University, Liaocheng 252000, P.R. China

*Corresponding Authors. E-mail: liuyifei@jlu.edu.cn, ttlin@jlu.edu.cn, zoubo@jlu.edu.cn

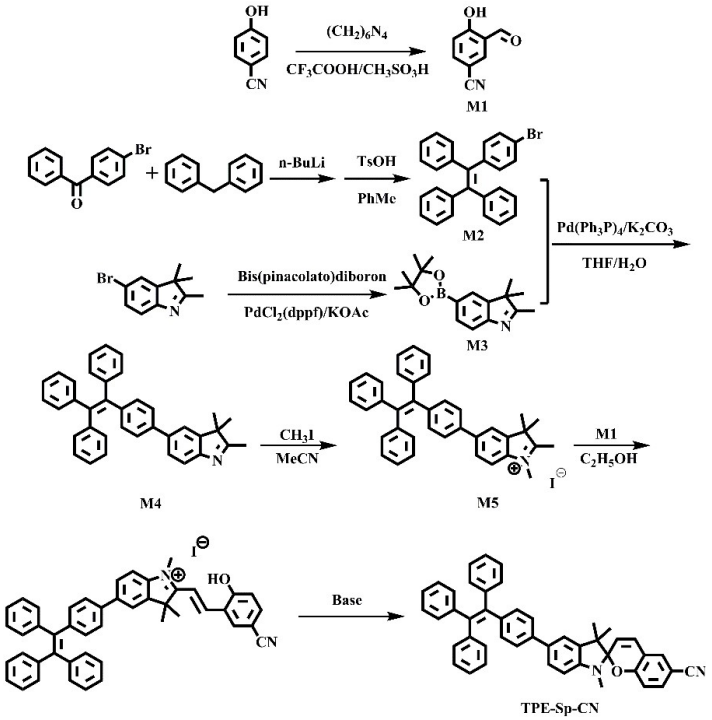

Scheme S1. The synthetic route of TPE-Sp-CN.

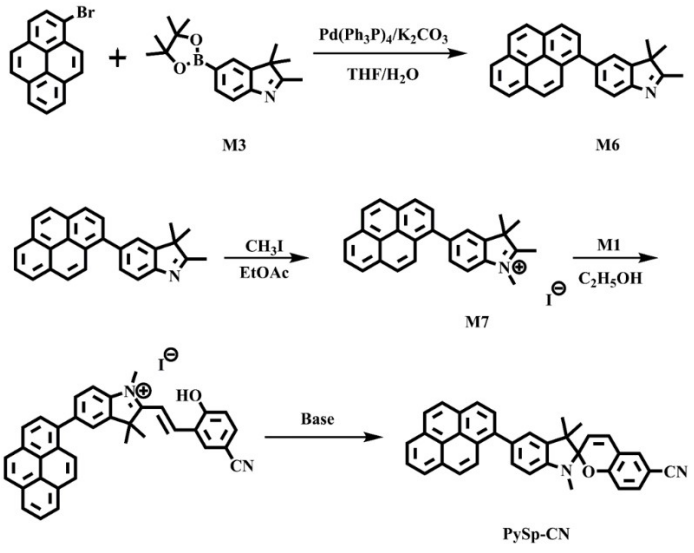

Scheme S2. The synthetic route of Py-Sp-CN.

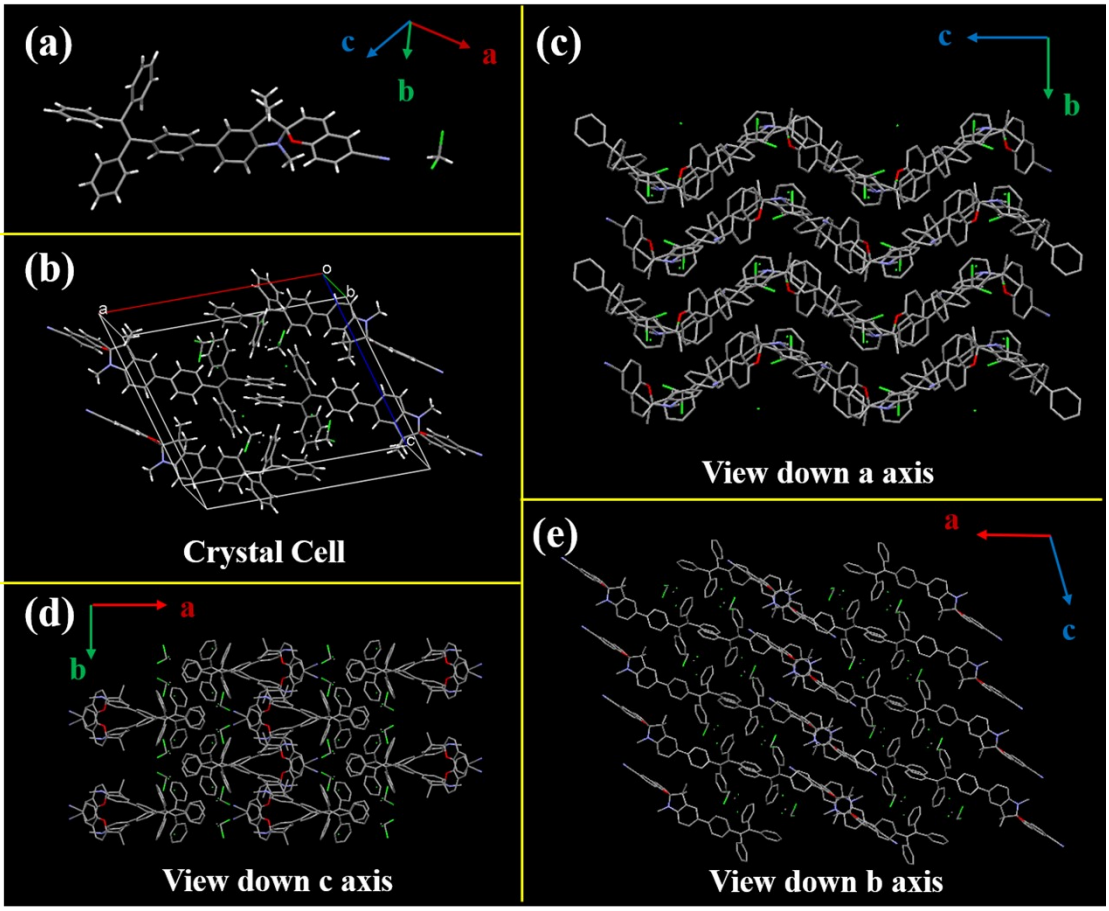

Fig. S1 (a) The molecular structure of TPE-Sp-CN in single crystal. (b) The unit cell of TPE-Sp-CN single crystal, and the packing patterns viewed down (c) a axis, (d) c axis and (e) b axis, respectively.

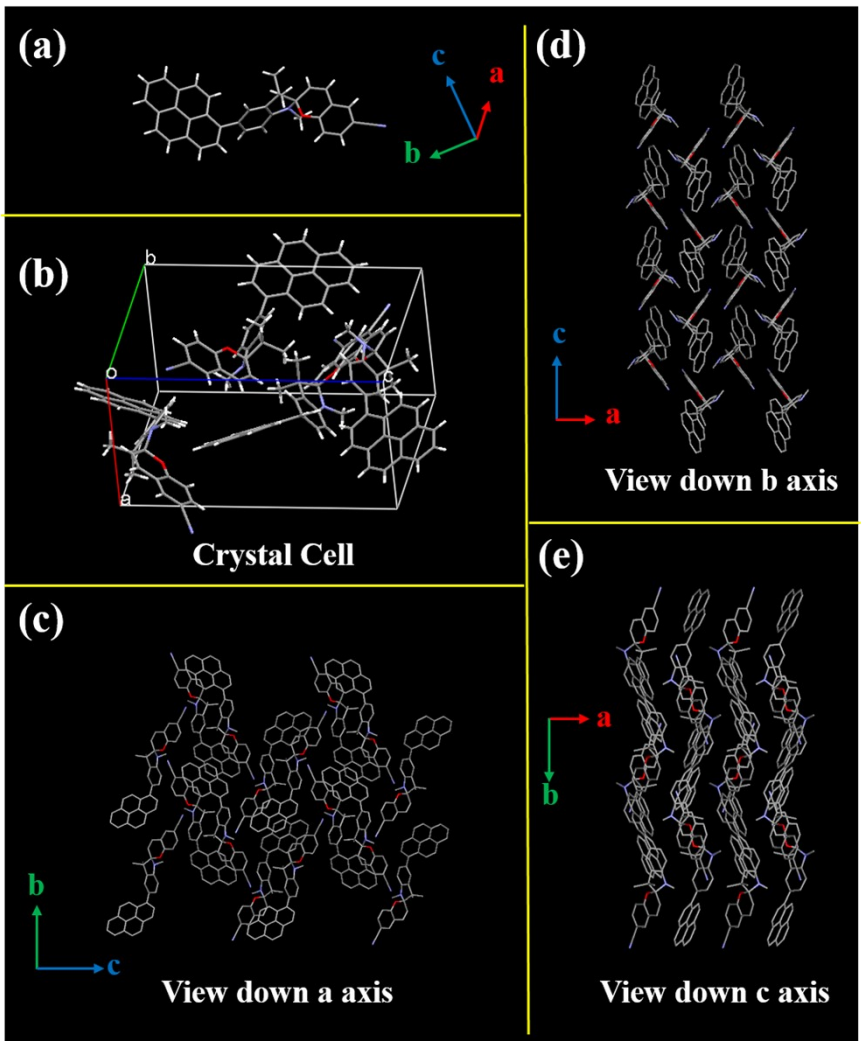

Fig. S2 (a) The molecular structure of Py-Sp-CN in single crystal. (b) The unit cell of Py-Sp-CN single crystal, and the packing patterns viewed down (c) a axis, (d) b axis and (e) c axis, respectively.

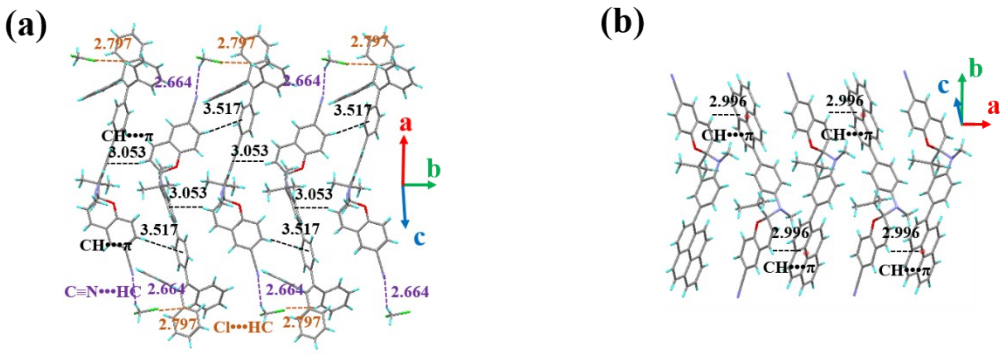

Fig. S3 Illustration of intermolecular interactions of (a) cTPE-Sp-CN and (b) cPy-Sp-CN.

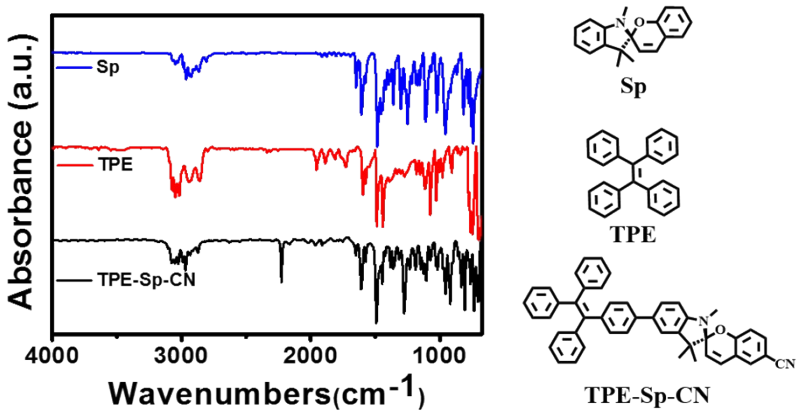

Fig. S4 The IR spectra of TPE-Sp-CN and corresponding fragments. IR spectra of spiropyran (Sp), tetraphenylethene (TPE) and TPE-Sp-CN.

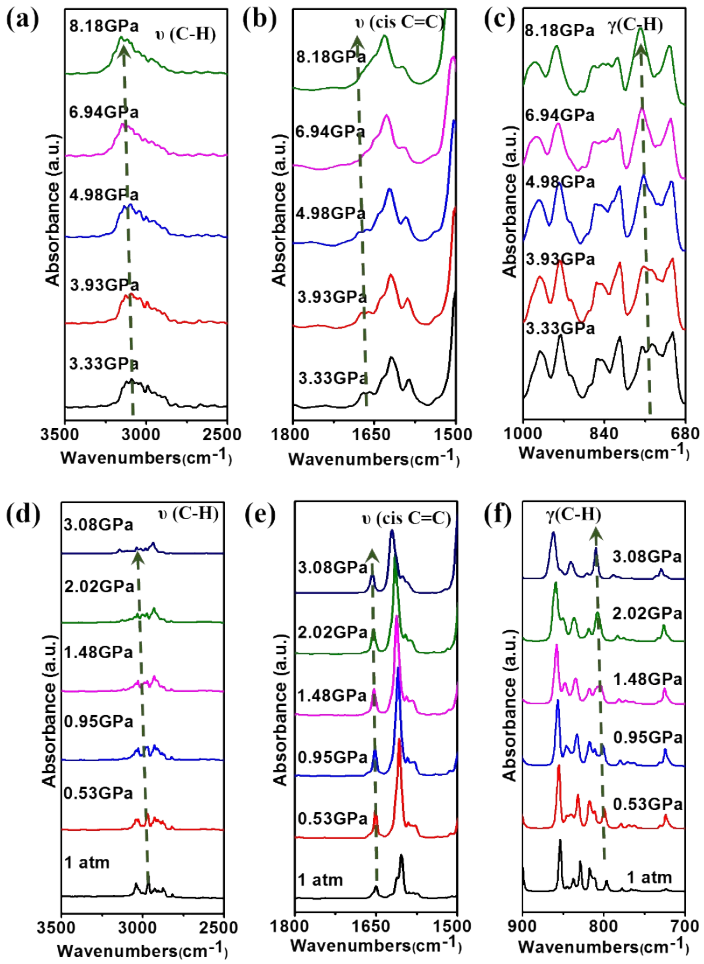

Fig S5 High-pressure IR spectra of (a-c) cTPE-Sp-CN and (d-f) cPy-Sp-CN in the regions of υ(C-H), υ(*cis* C=C) and γ(C-H) vibration modes.

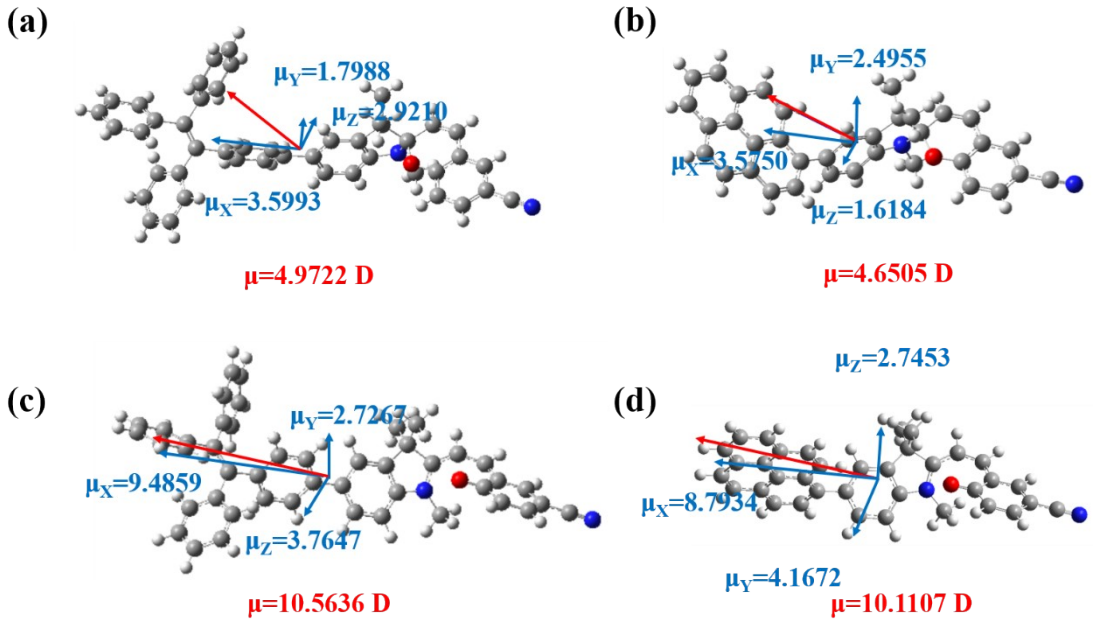

Fig. S6 The dipole moment calculations for ring closed and *cis*-structure of TPE and pyrene decorated spiropyrans. The dipole moments of (a) TPE-Sp-CN and (b) Py-Sp-CN in single crystal. The dipole moments of optimized (c) TPE-MC-CN-*cis* and (d) Py-MC-CN-*cis*. All the dipole moments were calculated by Gaussian 09 with basis set of B3LYP/6-31G (d).

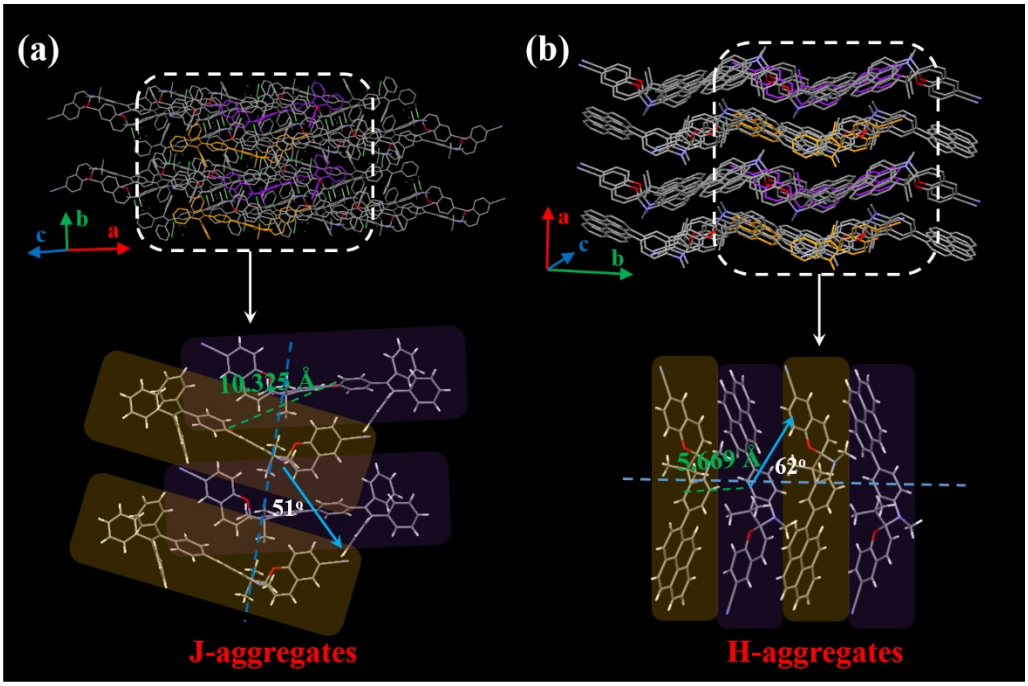

Fig. S7 The geometric central distances of molecules in (a) cTPE-Sp-CN and (b) cPy-Sp-CN. Slip angles are about 51° and 62° for TPE-Sp-CN and Py-Sp-CN, respectively. (J-aggregates: slip angle<54.7°, H-aggregates: slip angle>54.7°)

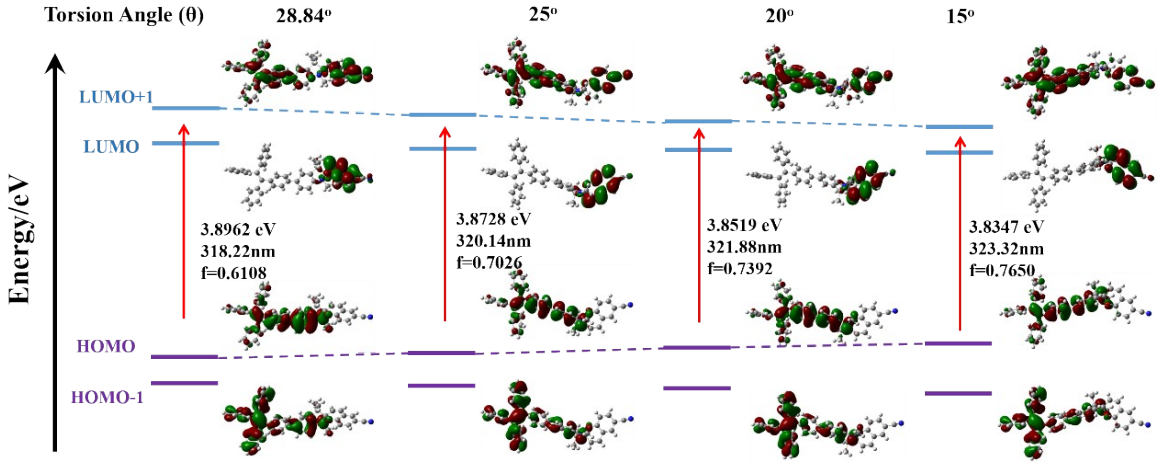

Fig. S8 The orbital amplitude plots and corresponding band gaps of TPE-Sp-CN in fixed conformation with gradually decreased torsion angels (θ) between TPE and spiropyran moieties. The plots were depicted by Gaussian 09 with basis set of B3LYP/6-31G (d), and f is the oscillator strength.

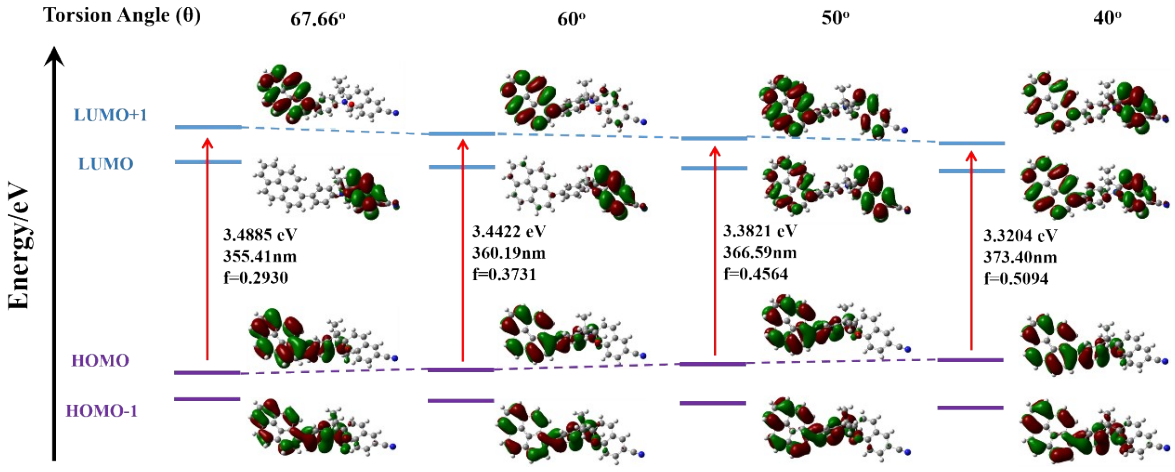

Fig. S9 The orbital amplitude plots and corresponding band gaps of Py-Sp-CN in fixed conformation with gradually decreased torsion angels (θ) between pyrene and spiropyran moieties. The plots were depicted by Gaussian 09 with basis set of B3LYP/6-31G (d), and f is the oscillator strength.

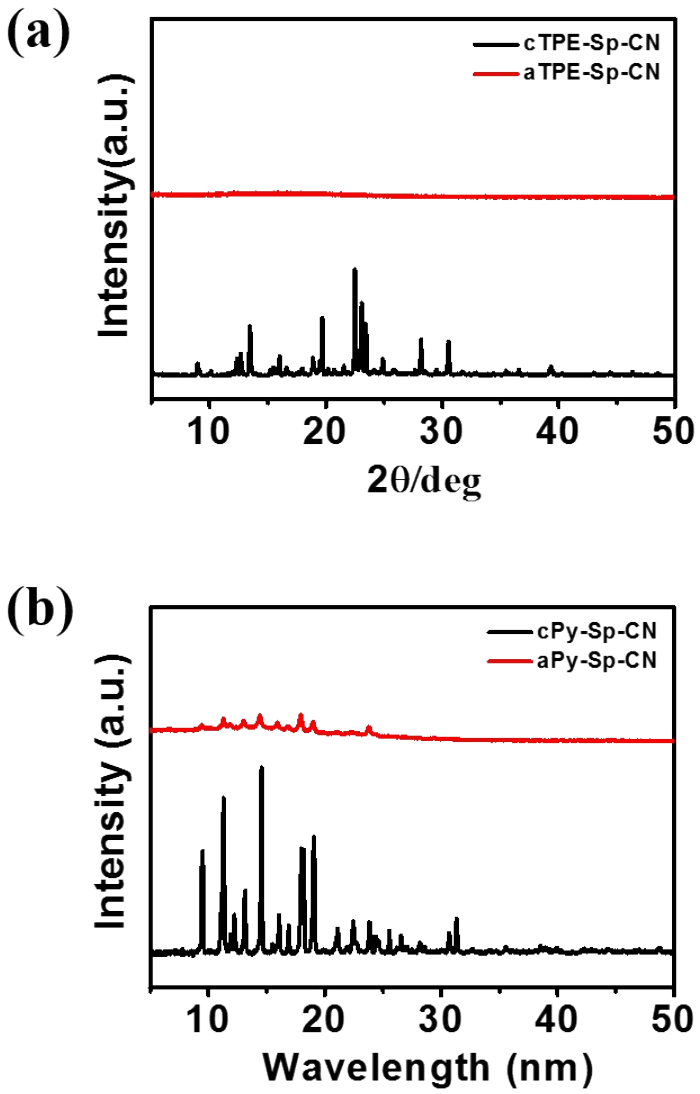

Fig. S10 (a) XRD patterns of cTPE-Sp-CN and aTPE-Sp-CN, (b) XRD patterns of cPy-Sp-CN and aPy-Sp-CN. The reduction and disappearance of XRD peaks meant that the crystal states changed into amorphous states.

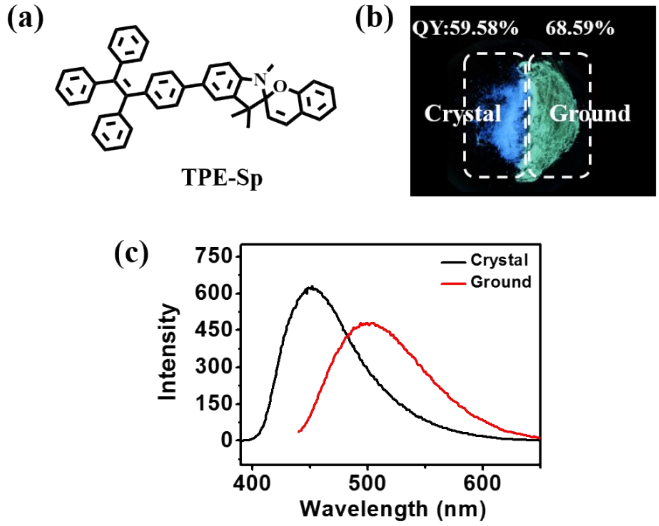

Fig. S11 (a) The structure of TPE-Sp, (b) fluorescent images and (c) PL spectra of TPE-Sp crystal before and after grinding treatment. The corresponding quantum yield (QY) were depicted in fluorescent images.

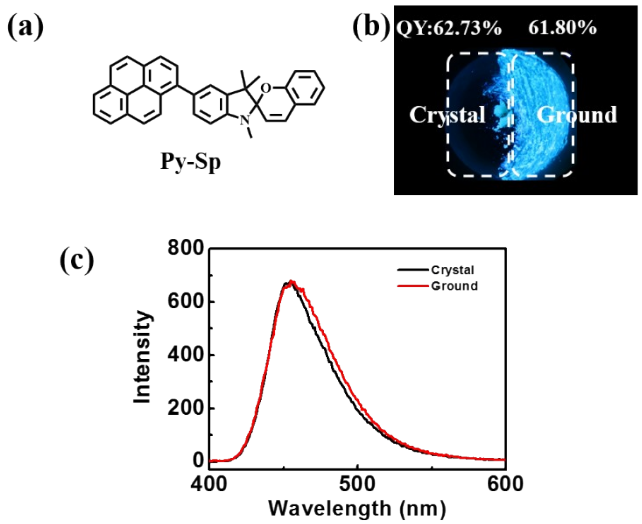

Fig. S12 (a) The structure of Py-Sp, (b) fluorescent images and (c) PL spectra of Py-Sp crystal before and after grinding treatment. The corresponding quantum yield (QY) were depicted in fluorescent images.

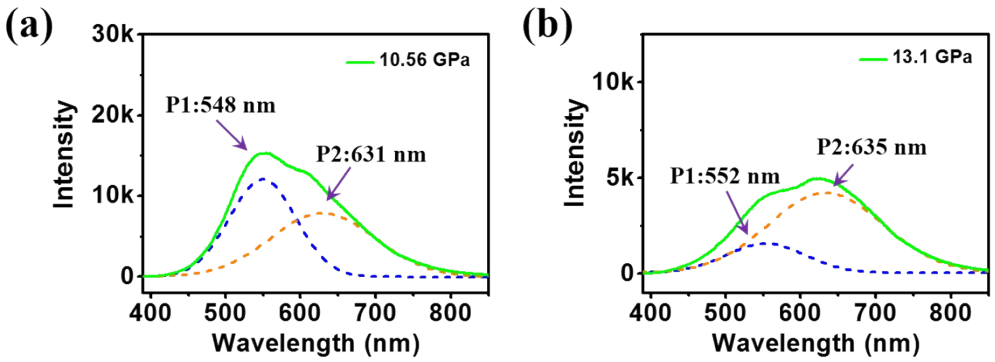

Fig. S13 The peak fittings of PL spectra of cTPE-Sp-CN at (a) 10.56 GPa (Adj. R-Square=0.996539) and (b) 13.1 GPa (Adj. R-Square=0.996653) in pressurization process.

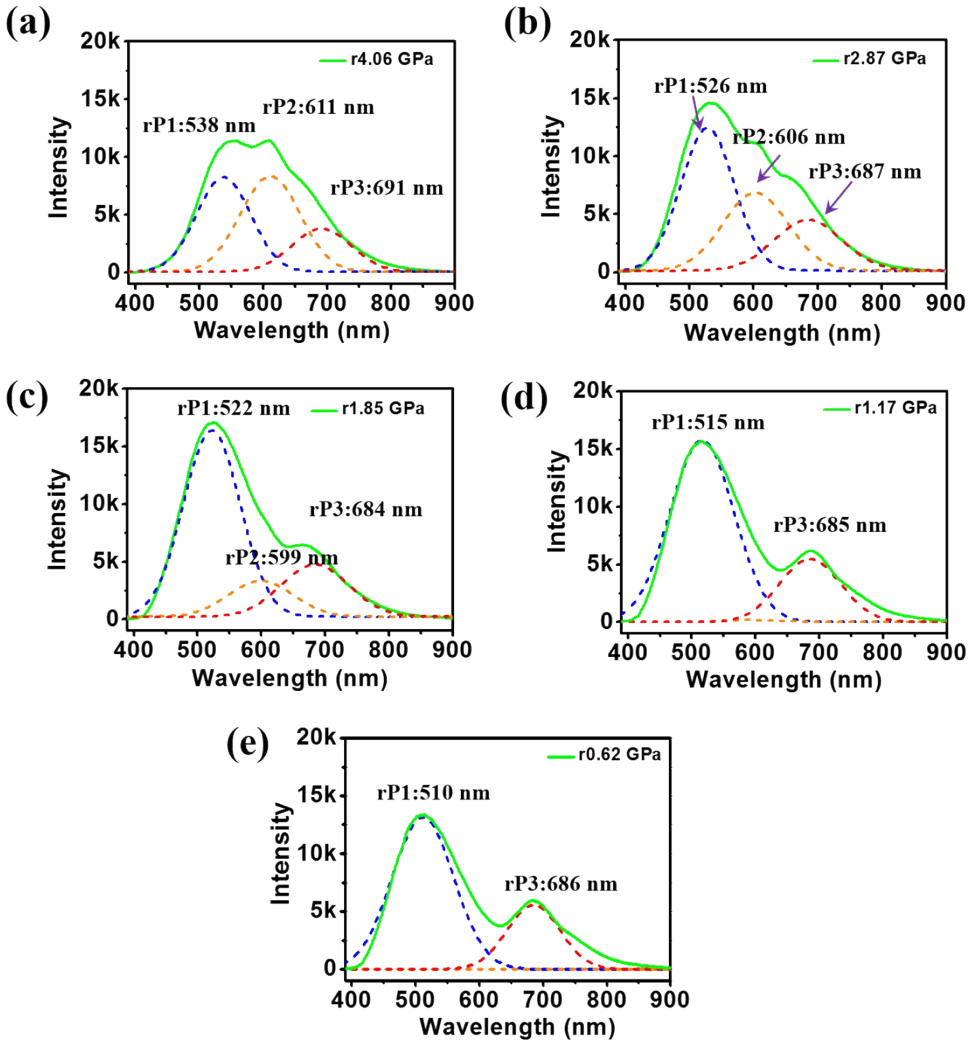

Fig. S14 The peak fittings of PL spectra of cTPE-Sp-CN at (a) 4.06 GPa (Adj. R-Square=0.995115), (b) 2.87 GPa (Adj. R-Square=0.993276), (c) 1.85 GPa (Adj. R-Square=0.995217), (d) 1.17 GPa (Adj. R-Square=0.992199), (e) 0.62 GPa (Adj. R-Square=0.993325) in the depressurization process.

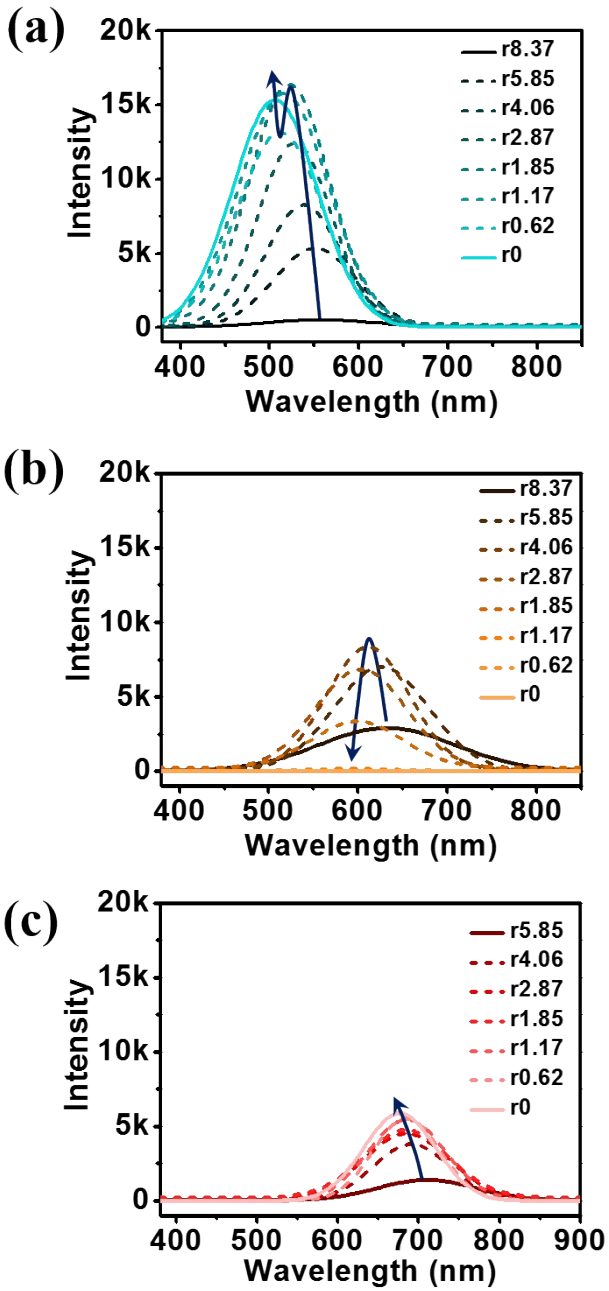

Fig. S15 The PL spectra of (a) rP1, (b) rP2 and (e) rP3 after peak fitted with decreasing pressure, respectively.

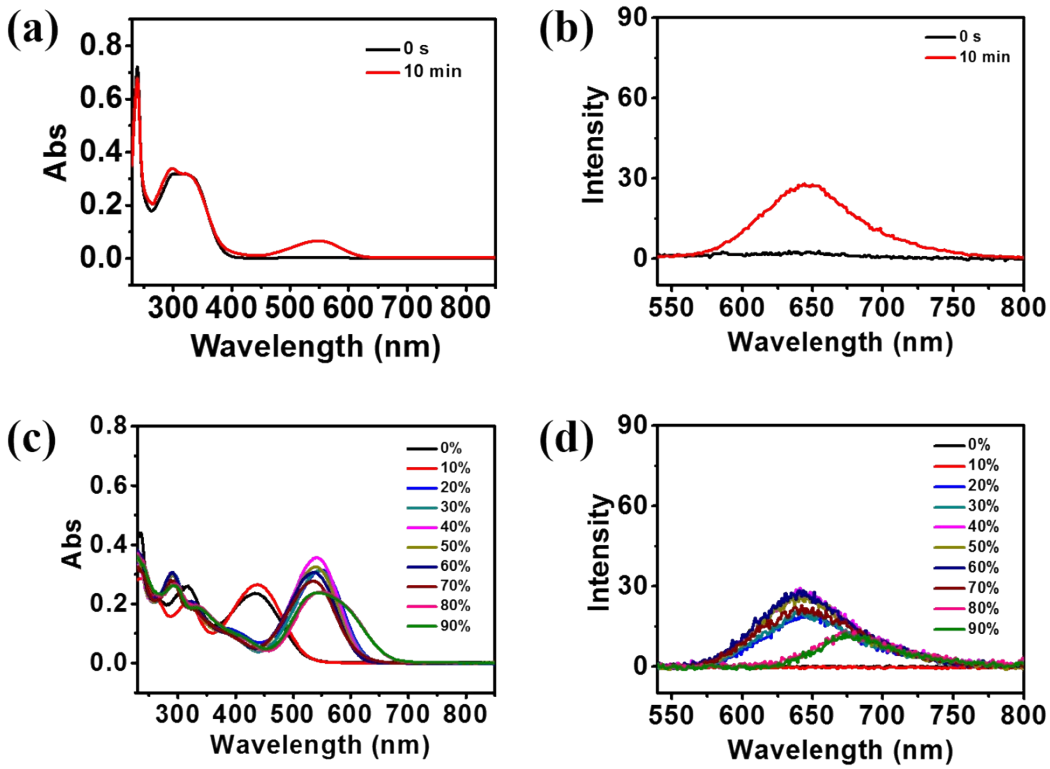

Fig. S16 (a) Absorption spectra and (b) PL spectra of TPE-Sp-CN solution (1×10^{-5} M, methanol) before and after treated with ten minutes of 254 nm UV light. (c) Absorption spectra and (d) PL spectra of TPE-MCH-CN (TPE-Sp-CN treated with 20 eq. HCl (2×10^{-4} M) to generate this protonated ring-open form, 1×10^{-5} M) in different volume fraction of MeCN/H_2O mixture, respectively. After UV light irradiation, TPE-Sp-CN switched to its non-protonated MC-*trans* form (TPE-MC-CN-*trans*), the absorption of TPE-MC-CN-*trans* is about 548 nm and the corresponding PL is located at about 646 nm. As for TPE-MCH-CN, when water fraction higher than 10% (20%-70%), TPE-MCH-CN lost proton, and TPE-MC-CN-*trans* formed since the absorption red shifted from 438 nm to about 550 nm, the corresponding emissions were about 644 nm, which is similar to the UV light induced TPE-MC-CN-*trans*. When the water fraction further increased to 80% and 90%, aggregation of TPE-MC-CN-*trans* generated, and the corresponding emission further red shifted to 676 nm. This indicates that the emission at 677 nm in Fig. 4c should originate from TPE-MC-CN-*trans*.

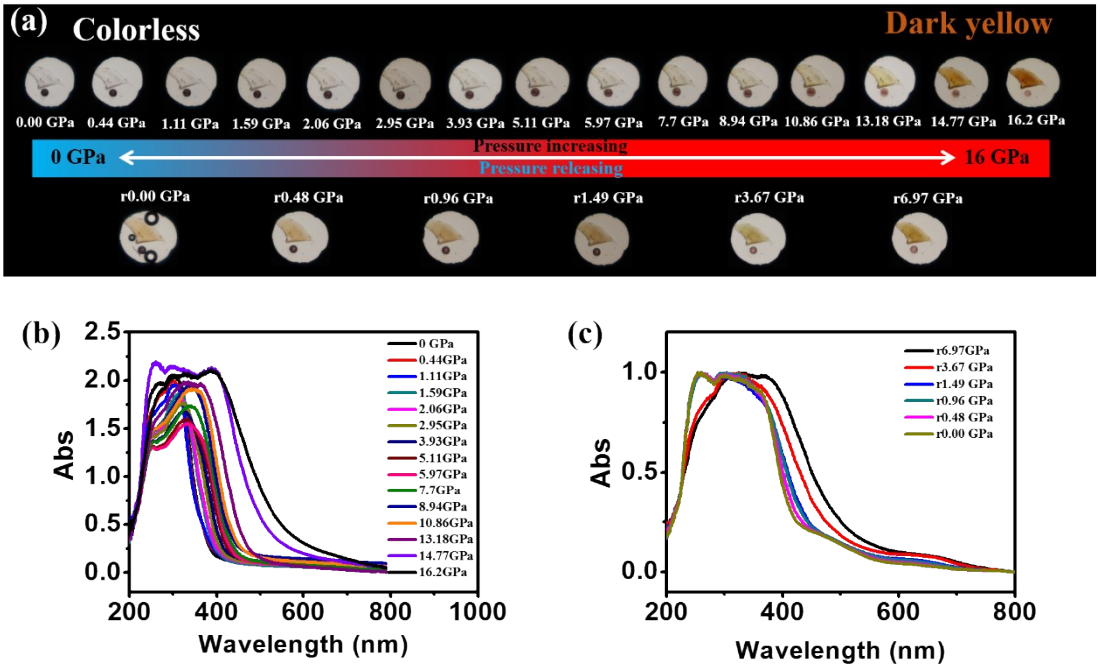

Fig. S17 (a) The pictures of cTPE-Sp-CN in the pressurizing and depressurizing process under ambient light. The in situ absorption spectra of cTPE-Sp-CN in the (b) pressurizing process and (c) depressurizing process.

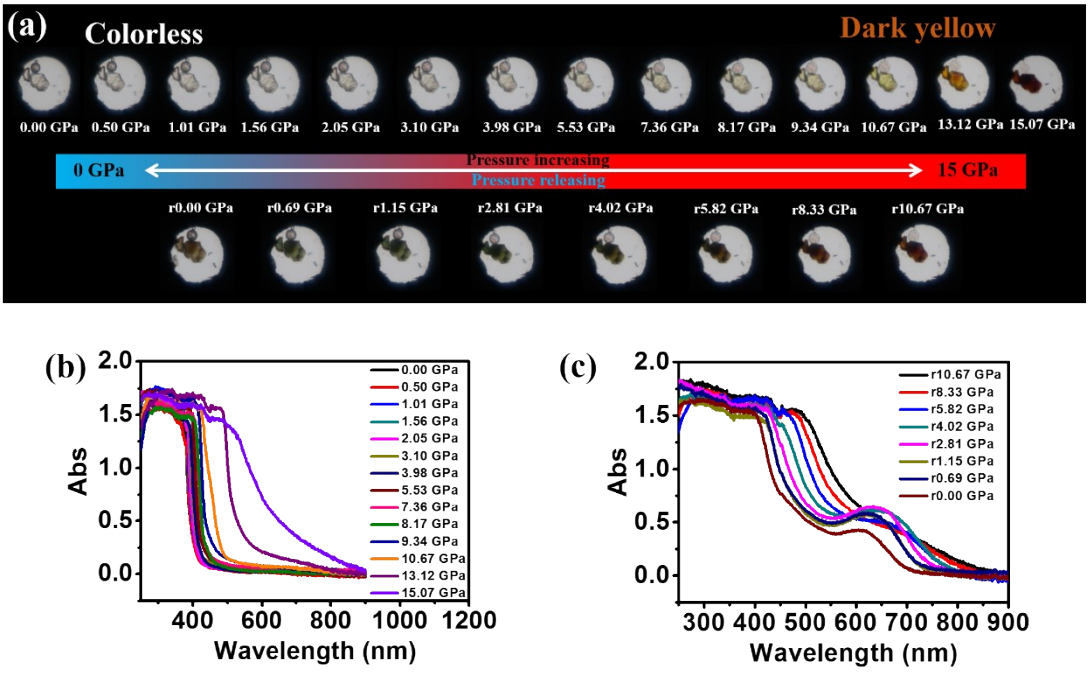

Fig. S18 (a) The pictures of cPy-Sp-CN in the pressurizing and depressurizing process under ambient light. The in situ absorption spectra of cPy-Sp-CN in the (b) pressurizing process and (c) depressurizing process.

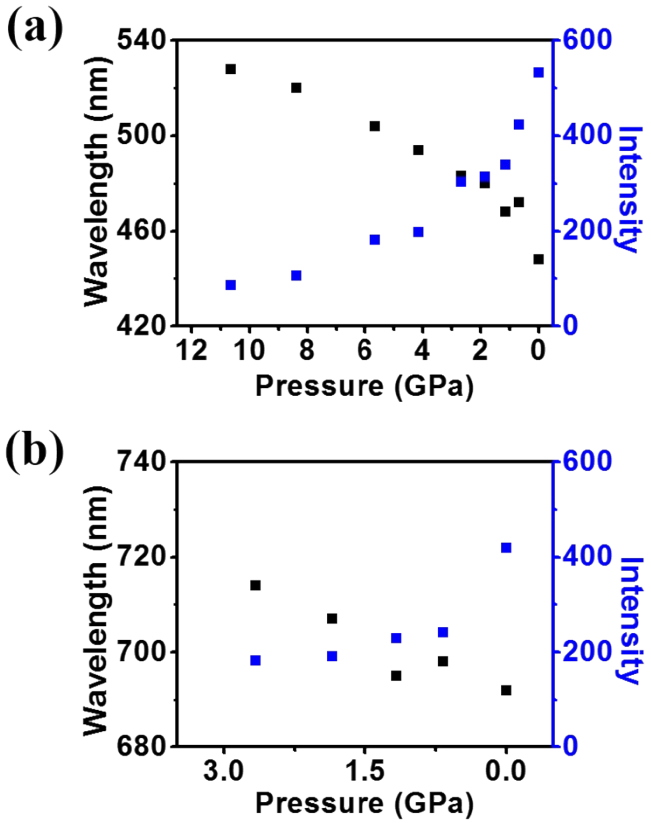

Fig. S19 The emissive changing trends of cPy-Sp-CN. The changing trends of wavelength and emissive intensity of (a) rP1' and (b) rP2' of cPy-Sp-CN with decreasing pressure, respectively.

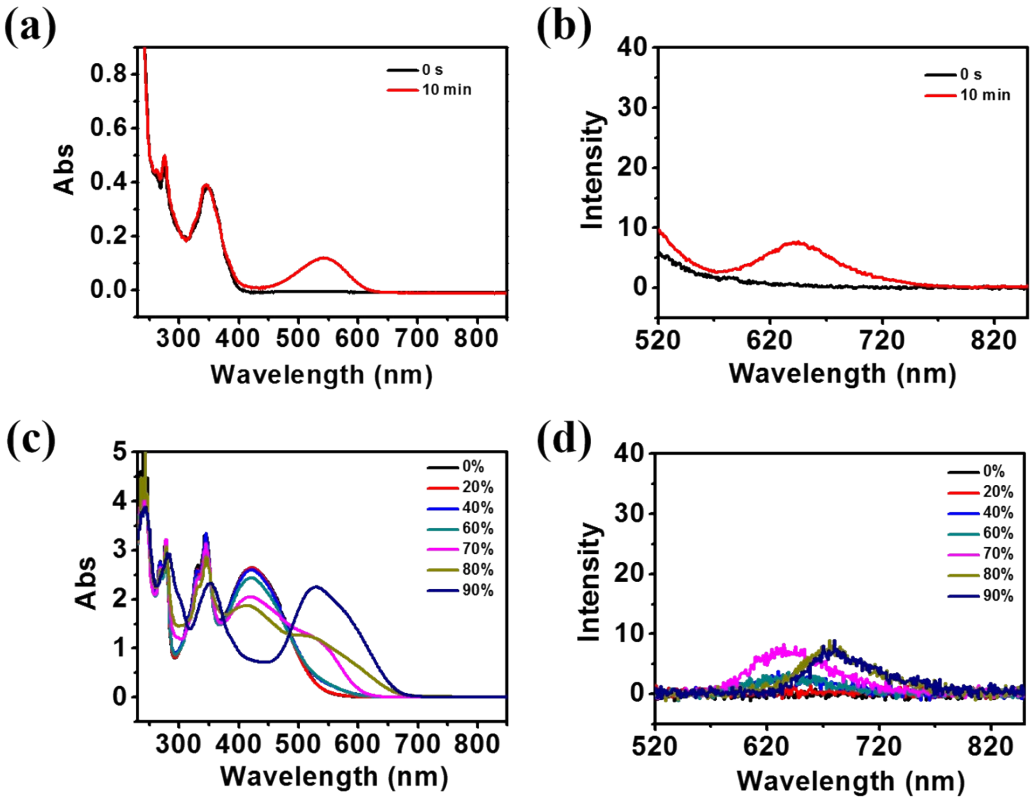

Fig. S20 (a) Absorption spectra and (b) PL spectra of Py-Sp-CN solution (1×10^{-5} M, methanol) before and after treated with ten minutes of 254 nm UV light. (c) Absorption spectra and (d) PL spectra of Py-MCH-CN (Py-Sp-CN treated with 2 eq. HCl (2×10^{-4} M) to generate this protonated ring-open form, 1×10^{-4} M) in different volume fraction of MeCN/H_2O mixture, respectively. After UV light irradiation, Py-Sp-CN switched to its non-protonated MC-*trans* form (Py-MC-CN-*trans*), the absorption of Py-MC-CN-*trans* is at about 545 nm and the corresponding PL located at about 644 nm. Similar to the TPE-MCH-CN system, when water fraction reach 80% and 90%, obvious deprotonation process occurred as the absorption peak at about 541 nm appeared, and the emission of Py-MC-CN-*trans* aggregates red shifted from 641 nm to 681 nm. This indicates that the emission at 692 nm in Fig. 4c should originate from Py-MC-CN-*trans*.

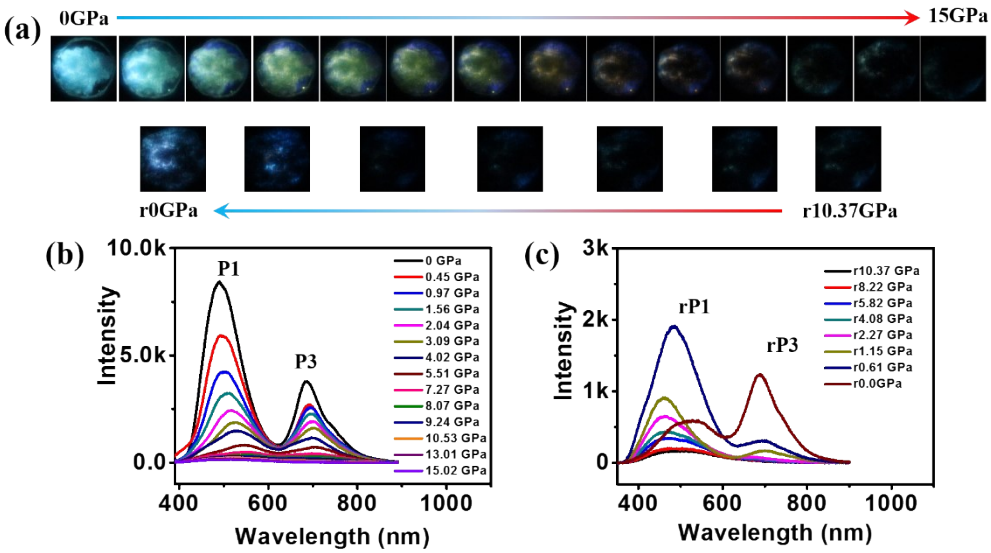

Fig. S21 (a) Fluorescent images of amorphous TPE-Sp-CN in the pressurizing and depressurizing process. (b) PL spectra of amorphous TPE-Sp-CN with increasing hydrostatic pressure. (c) PL spectra of amorphous TPE-Sp-CN with decreasing hydrostatic pressure.

In order to obtain completely amorphous state, elaborative machine-grinding was exerted to cTPE-Sp-CN. While under high shear force, partial TPE-Sp-CN was switched to MC-*trans* form (TPE-MC-CN-*trans*), and the P3 was found at 0 GPa (Fig. S21b). Throughout the pressurizing process (0 GPa~15GPa) and depressurizing process (15 GPa~r0 GPa), only P1, P3, rP1 and rP3 can be found. This means that without suitable intermolecular interactions and topological structure, the ultra-unstable MC-*cis* form (TPE-MC-CN-*cis*) couldn't be captured.

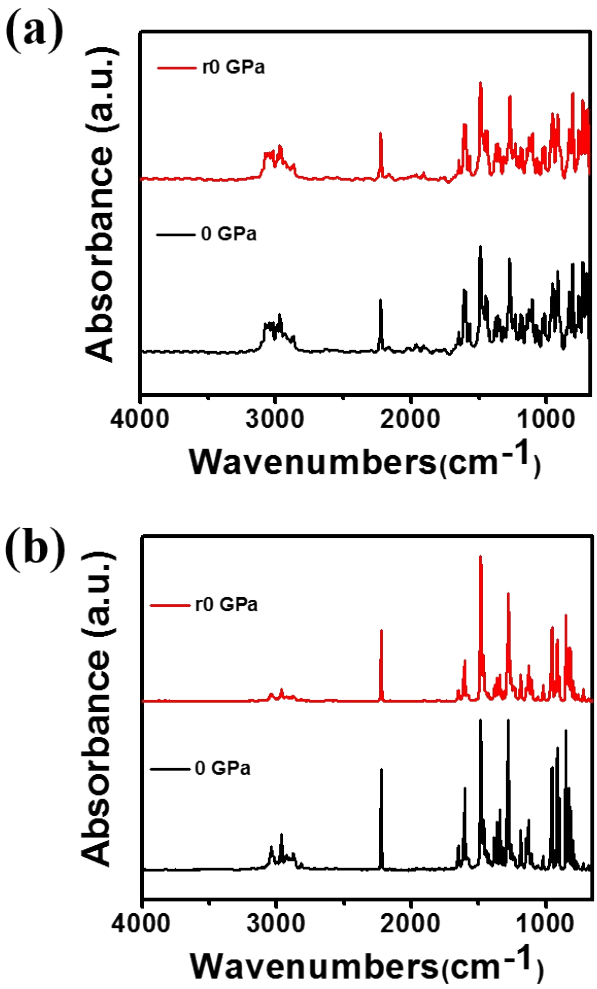

Fig. S22 The IR spectra of (a) cTPE-Sp-CN and (b) cPy-Sp-CN before pressure was exerted and after pressure was released.

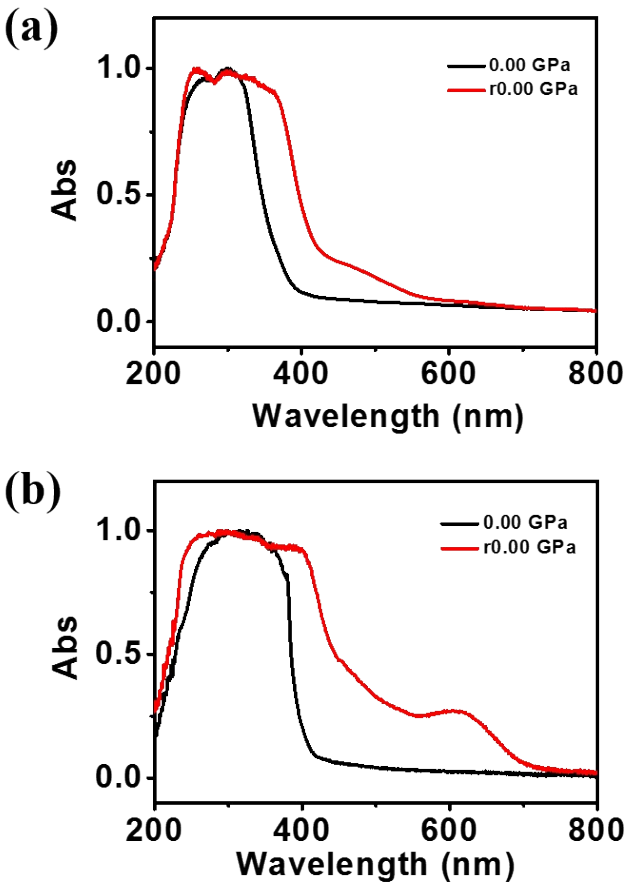

Fig. S23 The absorption spectra of (a) cTPE-Sp-CN and (b) cPy-Sp-CN before pressure was exerted and after pressure was released.

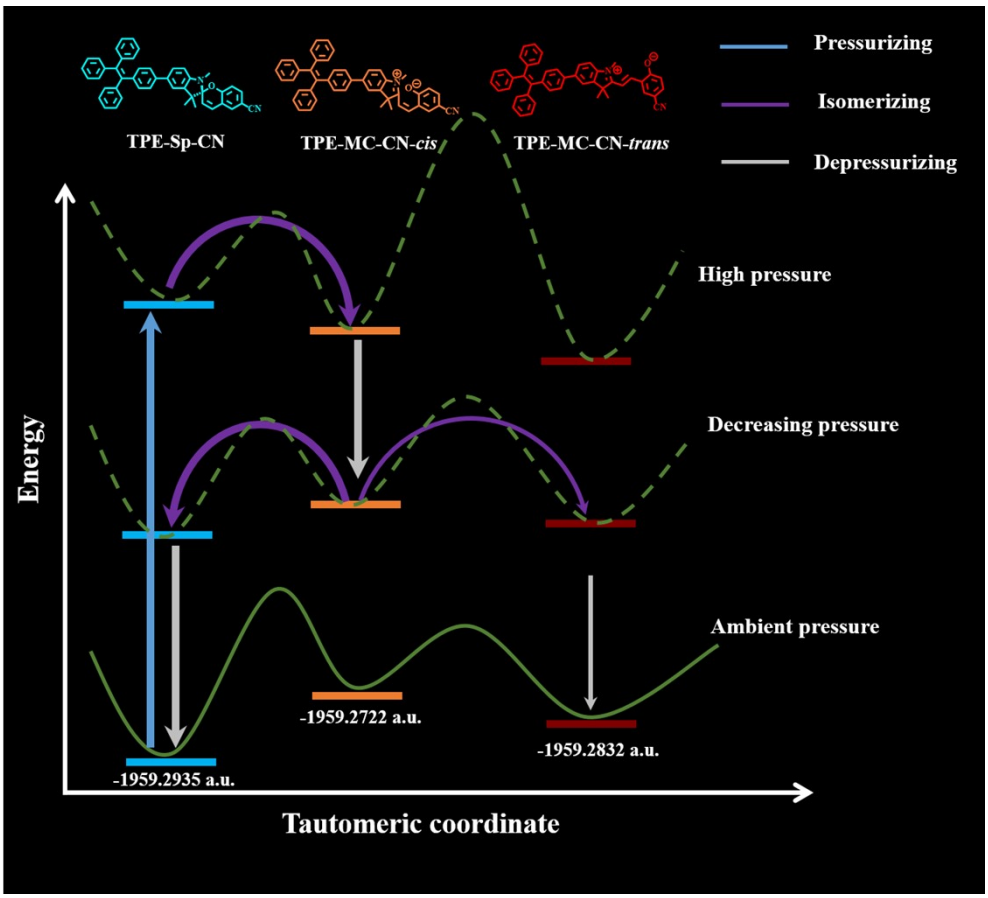

Fig. S24 The proposed potential energy diagram of TPE-Sp-CN, TPE-MC-CN-*cis* and TPE-MC-CN-*trans* under low pressure and high pressure.

Table S1. The quantum yields, lifetimes, irradiation rate and non-irradiation rates of cTPE-Sp-CN, aTPE-Sp-CN, cPy-Sp-CN and aPy-Sp-CN.

Sample	Φ_f (%)	τ_1	τ_2	K_r	K_{nr}
cTPE-Sp-CN	6.15%	1.40 ns (34.02%)	3.04 ns (65.98%)	2.477×10^7 s^{-1}	3.781×10^8 s^{-1}
aTPE-Sp-CN	34.62%	1.47 ns (41.29%)	3.61 ns (58.71%)	1.270×10^8 s^{-1}	2.398×10^8 s^{-1}
cPy-Sp-CN	2.22%	0.94 ns (70.55%)	2.80 ns (29.45%)	1.492×10^7 s^{-1}	6.572×10^8 s^{-1}
aPy-Sp-CN	7.10%	1.00 ns (72.43%)	3.73 ns (27.57%)	4.051×10^7 s^{-1}	5.300×10^8 s^{-1}

NMR and Mass spectra

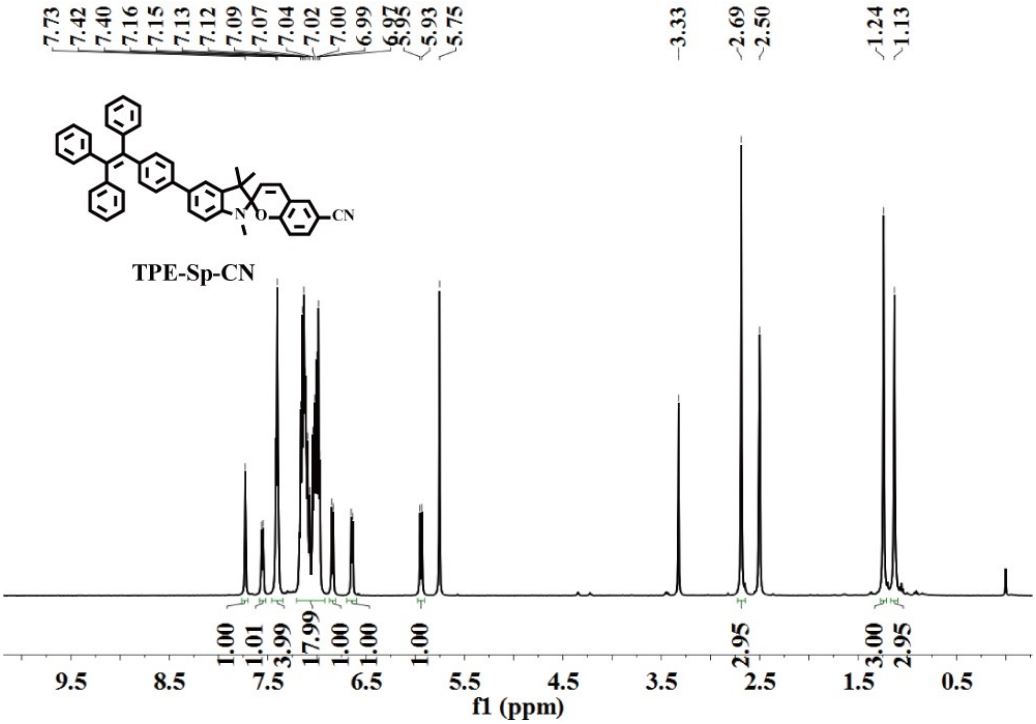

Fig. 25 ^{1}H NMR spectrum of TPE-Sp-CN in DMSO-d_6.

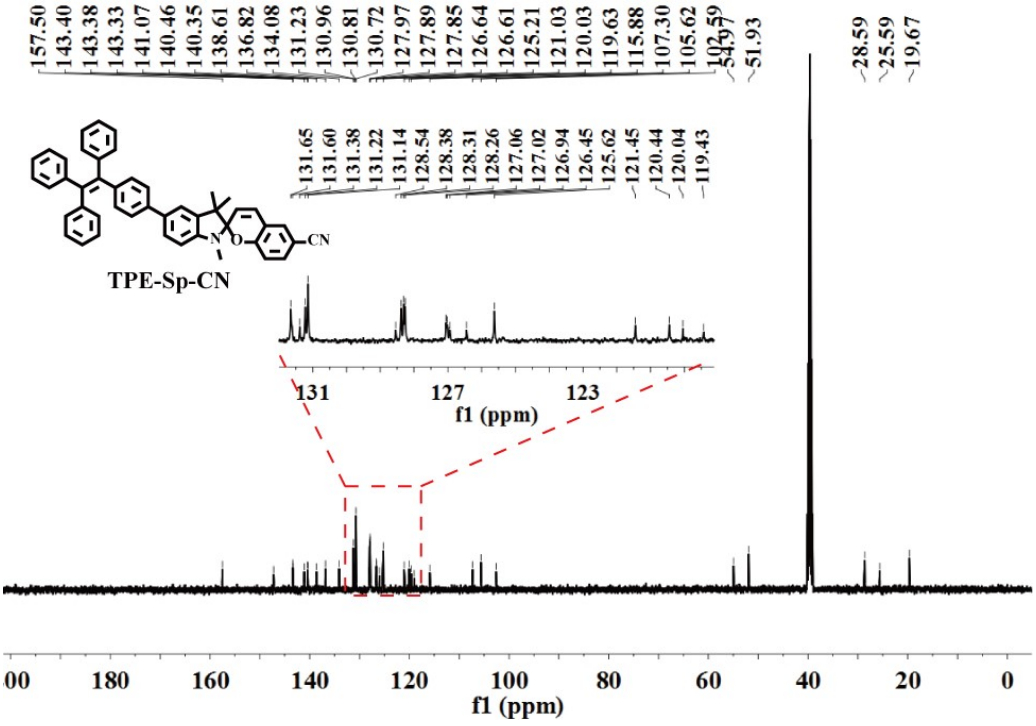

Fig. S26 ^{13}C NMR spectrum of TPE-Sp-CN in DMSO-d_6.

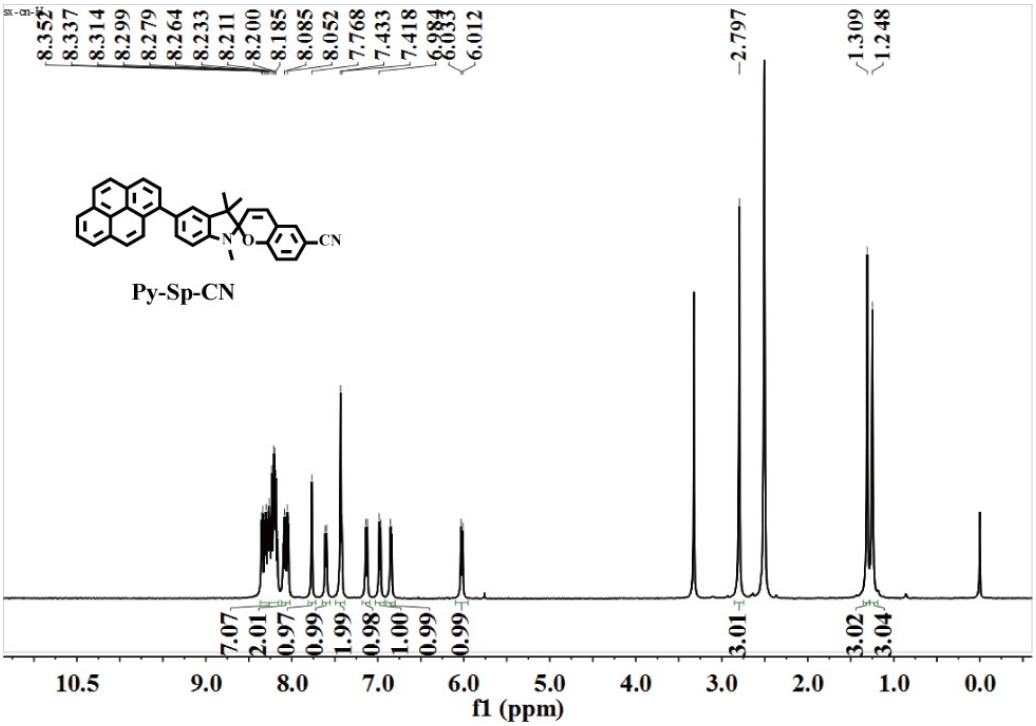

Fig. S27 [1]H NMR spectrum of Py-Sp-CN in DMSO-d_6.

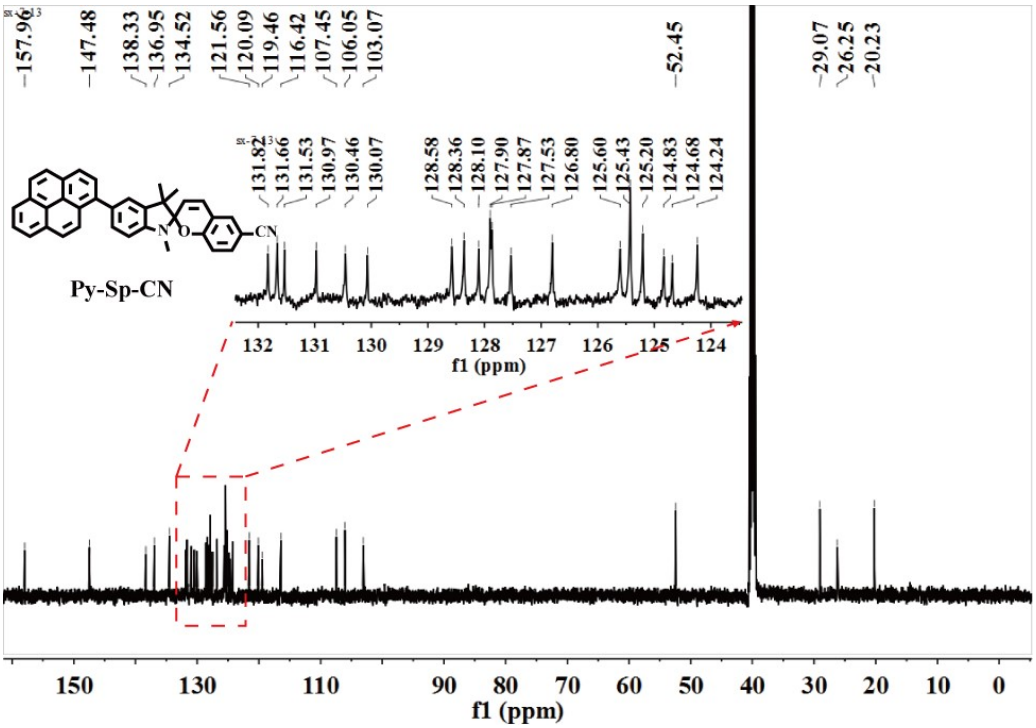

Fig. S28 [13]C NMR spectrum of Py-Sp-CN in DMSO-d_6.

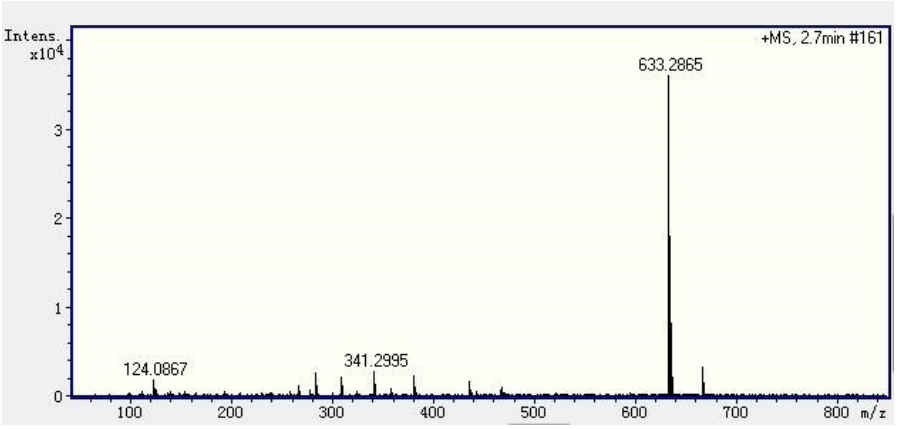

Fig. S29 MS spectrum of TPE-Sp-CN.

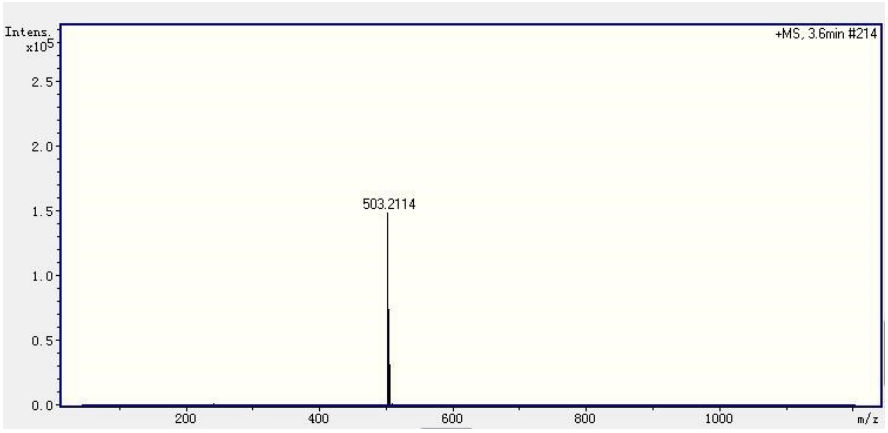

Fig. S30 MS spectrum of Py-Sp-CN.

Crystal data

Crystal data: [CCDC 1821887, 1900159 contains the supplementary crystallographic data for this the crystal of TPE-Sp-CN and Py-Sp-CN, respectively. These data can be obtained free of charge from The Cambridge Crystallographic Data Centre via www.ccdc.cam.ac.uk/data_request/cif.]

Table S2. Crystal data and structure refinement for TPE-Sp-CN.

Identification code	TPE-Sp-CN
Empirical formula	$C_{47}H_{38}Cl_2N_2O$
Formula weight	717.69
Temperature	273(2) K
Wavelength	0.71073 Å
Crystal system, space group	Monoclinic, *P*21/c
Unit cell dimensions	*a*= 20.728(9) Å *α*= 90°
	b= 11.337(5) Å *β*= 107.633(8)°
	c= 17.818(8) Å *γ*= 90°
Volume	3990(3) Å^3
Z, Calculated density	4, 1.195 g/cm^{-3}
Absorption coefficient	0.200 mm^{-1}
F(000)	1504.0
Crystal size	0.22× 0.20× 0.18 mm^3
Theta range for data collection	1.03 to 25.00°
Limiting indices	$-22\le h\le 24$, $-11\le k\le 13$, $-21\le l\le 20$
Reflections collected / unique	22165 / 6987 [R_{int}= 0.1070]
Completeness to theta = 25.00	99.3%
Absorption correction	Multi-scan
Max. and min. transmission	0.9649 and 0.9574

Refinement method	Full-matrix least-squares on F^2
Data / restraints / parameters	6987 / 61 / 501
Goodness-of-fit on F^2	0.890
Final R indices [I>2σ(I)][a]	$R1$= 0.0866, $wR2$= 0.2215
R indices (all data)	$R1$= 0.2198, w$R2$= 0.2971
Extinction coefficient	0.0053(11)
Largest diff. peak and hole	0.533 and -0.324 e.Å^{-3}

Table S3. Crystal data and structure refinement for Py-Sp-CN.

Identification code	Py-Sp-CN
Empirical formula	$C_{36}H_{26}N_2O$
Formula weight	502.59
Temperature	299.73 K
Wavelength	0.71073 Å
Crystal system, space group	Orthorhombic, $P2_12_12_1$
Unit cell dimensions	a= 9.9020(5) Å α= 90°
	b= 14.4344(9) Å β= 90°
	c= 18.7537(11) Å γ= 90°
Volume	2680.5(3) Å^3
Z, Calculated density	4, 1.245 g/cm^{-3}
Absorption coefficient	0.075 mm^{-1}
F(000)	1056
Crystal size	0.05× 0.04× 0.03 mm^3
Theta range for data collection	2.721 to 27.468°
Limiting indices	$-12\leq h\leq 10$, $-18\leq k\leq 18$, $-24\leq l\leq 24$
Reflections collected / unique	32303 / 6142 [R_{int}= 0.0387]
Completeness to theta = 25.00	99.8%
Absorption correction	Semi-empirical from equivalents
Max. and min. transmission	0.7456 and 0.6780
Refinement method	Full-matrix least-squares on F^2
Data / restraints / parameters	6142 / 0 / 355
Goodness-of-fit on F^2	1.036
Final R indices [I>2σ(I)][a]	$R1$= 0.0458, $wR2$= 0.0949
R indices (all data)	$R1$= 0.0730, w$R2$= 0.1074
Extinction coefficient	n/a
Largest diff. peak and hole	0.119 and -0.139 e.Å^{-3}